

# MESH TYPE ANALYSIS FOR SIMULATING CAVITATION PHENOMENA IN INJECTION NOZZLE: THEORETICAL AND NUMERICAL ANALYSIS

*Blaž Vajda<sup>1</sup>, Zoran Žunič, Breda Kegl*

UDC: 621.43 :519.6

## INTRODUCTION

The development of the modern compression ignition engine is mainly connected with rising of injection pressure and the possibility of the injecting several jets during the single injection cycle. Both modifications influence positively the engine characteristics and the emission formation processes. On the other side rising of the injection pressure results in higher flow velocities in the nozzle hole channels and in evaporation of fuel in the nozzle holes. The fuel evaporates on the sharp edge at the nozzle inlet, where the static pressure falls below the fuel vapour pressure. The vapour is spreading along the nozzle hole and could also reach the outlet. The evaporation of fuel and cavitation process in the nozzle hole significantly influence the in-nozzle flow and spray formation process.

## THEORETICAL BACKGROUNDS

Cavitation bubbles form because of low static pressure that occurs near a sharp inlet corner in the nozzle flow. If the corner of the inlet is sufficiently sharp, the flow tends to separate and form a contraction inside the nozzle, which reduces the area through which the liquid flows. This reduced area is accompanied by increase in velocity, as predicted by conservation of mass. Conservation of momentum predicts that the acceleration of the liquid through the vena contracta causes a pressure depression in the throat of the nozzle. The low pressure inside the throat of the nozzle may fall below the vapour pressure of the liquid, causing cavitation. Cavitation flow does not, however, strictly adhere to this simple idealization. The formation of the bubbles is sensitive to the geometry of corner and any imperfections in the nozzle shape. The cavitation is also very sensitive to the quality of the liquid. Furthermore, cavitation inception may occur at pressure below the vapour pressure. Another complication is that the cavitating flow is transient and fully three-dimensional. The location of the vapour is not steady and it is usually also not symmetrical.

### Nozzle geometry

Analyses were made for one-hole nozzle with sac volume and sharp edges at the nozzle hole inlet side. Dimension of the tested nozzle are presented in Table 1.

---

<sup>1</sup> Corresponding author e-mail: [blaz.vajda@uni-mb.si](mailto:blaz.vajda@uni-mb.si), University of Maribor, Faculty of mechanical engineering, Engine research Laboratory, Smetanova ulica 17, SI-2000 Maribor, Slovenia

**Table 1:** Nozzle dimensions

Nozzle hole diameter	$d_d$	0,68 mm
Nozzle hole channel length	$l_s$	1 mm
Sac chamber diameter	$D_E$	1,5 mm
Needle seat diameter	$D_A$	1,36
Needle tip cone angle	$\alpha$	120°
Needle seat cone angle	$\sigma$	60°
Maximal needle lift	$h_{mx}$	0,30 mm

### Flow coefficient definitions

Flow coefficient, despite its simplicity, represent one of the most important values, representing the fuel injection conditions at the nozzle. It is defined as ratio between the measured or real ( $V_{real}$ ) and theoretical ( $V_{th}$ ) volume flow injected through the nozzle. According to Bernoulli equation, the theoretical outflow velocity can be derived from the pressure difference ( $\Delta p$ ) and fuel density ( $\rho$ ):

$$\mu = \frac{\dot{V}_{real}}{\dot{V}_{th}} = \frac{\dot{V}_{real}}{A_d \cdot \sqrt{\frac{2 \cdot \Delta p}{\rho}}} \quad (1)$$

$A_d$  represents the sum of the nozzle hole cross-section area, while  $\rho$  is the density of the fluid. Following the presented equations, higher flow coefficient values result in bigger quantity of fuel injected per time unit, higher outflow velocities and better fuel spray atomization.

### NUMERICAL ANALYSIS

Numerical analyses were made using the CFD program FIRE. Two-phase flow is calculated with two-equation model, with a continuous liquid and a dispersed vapour phase.

Mass conservation equation:

$$\frac{\partial \alpha_k \rho_k}{\partial t} + \nabla \cdot \rho_k \mathbf{v}_k = \sum_{l=1; l \neq k}^N \Gamma_{kl} \quad (1)$$

$\alpha_k$  is volume fraction of phase k,  $\mathbf{v}_k$  is phase k velocity, and  $\Gamma_{kl}$  presents the interfacial mass exchange between phases k and l. The compatibility condition must be fulfilled:

$$\sum_{k=1}^n \alpha_k = 1 \quad (2)$$

Momentum conservation equation:

$$\begin{aligned} \frac{\partial \alpha_k \rho_k \mathbf{v}_k}{\partial t} + \nabla \cdot \rho_k \mathbf{v}_k \mathbf{v}_k = & -\alpha_k \nabla p + \nabla \alpha_k (\boldsymbol{\tau}_k + \mathbf{T}_k') + \\ & + \alpha_k \rho_k \mathbf{g} + \sum_{l=1; l \neq k}^N \mathbf{M}_{kl} + \mathbf{v}_k \sum_{l=1; l \neq k}^N \Gamma_{kl} \end{aligned} \quad (3)$$

where  $\mathbf{f}$  is the body force vector which comprises of gravity  $\mathbf{g}$ ;  $\mathbf{M}_{kl}$  represents the momentum interfacial interaction between phase  $k$  and  $l$ , and  $p$  is pressure. Pressure is assumed identical for all phases. The phase  $k$  shear  $\boldsymbol{\tau}_k$ , equals:

$$\boldsymbol{\tau}_k = \mu_k \left[ (\nabla \mathbf{v}_k + \nabla \mathbf{v}_k^t) - \frac{2}{3} \nabla \cdot \mathbf{v}_k \right] \quad (4)$$

$\mu_k$  is molecular viscosity. Reynolds stress  $\mathbf{T}_k^t$  equals:

$$\mathbf{T}_k^t = -\rho_k \overline{\mathbf{v}_k' \mathbf{v}_k'} = \mu_k \left[ (\nabla \mathbf{v}_k + \nabla \mathbf{v}_k^t) - \frac{2}{3} \nabla \cdot \mathbf{v}_k \right] - \frac{2}{3} \nabla \cdot \mathbf{v}_k \mathbf{I} \quad (5)$$

Turbulent viscosity is modelled as:

$$\mu_k^t = \rho_k C_\mu \frac{k_k^2}{\varepsilon_k} \quad (6)$$

Since the analyses in the present paper were made at constant temperature the enthalpy conservation equation will not be described in the details here.

Turbulent kinetic energy (TKE) conservation equation:

$$\begin{aligned} \frac{\partial \alpha_k \rho_k k_k}{\partial t} + \nabla \cdot \rho_k \mathbf{v}_k k_k \nabla \cdot \alpha_k \left( \mu_k + \frac{\mu_k'}{\sigma_k} \right) \nabla k_k + \alpha_k P_k + \alpha_k P_{B,k} - \\ - \alpha_k \rho_k \varepsilon_k + \alpha_k \frac{dp}{dt} + \sum_{l=1; l \neq k}^N K_{kl} + k_k \sum_{l=1; l \neq k}^N \Gamma_{kl} \end{aligned} \quad (7)$$

Turbulence dissipation equation (TED):

$$\begin{aligned} \frac{\partial \alpha_k \rho_k \varepsilon_k}{\partial t} + \nabla \cdot \rho_k \mathbf{v}_k k_k \nabla \cdot \alpha_k \left( \mu_k + \frac{\mu_k'}{\sigma_k} \right) \nabla \varepsilon_k + \alpha_k C_1 P_k \frac{\varepsilon_k}{k_k} + \alpha_k C_2 \rho_k \frac{k_k \varepsilon_k^2}{k_k} + \\ + \alpha_k C_3 \rho_k \max(P_{B,k}, 0) \frac{\varepsilon_k}{k_k} - \alpha_k C_4 \rho_k \varepsilon_k \nabla \cdot \mathbf{v}_k + \sum_{l=1; l \neq k}^N D_{kl} + \varepsilon_k \sum_{l=1; l \neq k}^N \Gamma_{kl} \end{aligned} \quad (8)$$

In two-equation model several mass exchange terms could be introduced (according to the type of two-phase flow). In the present analysis the cavitation model is employed.

Mass exchange term is defined with following equations

$$\Gamma_c = \frac{1}{C_{CR}} \text{sign}(\Delta p) \cdot 3,85 \cdot \frac{\rho_d}{\sqrt{\rho_c}} N'''^{1/3} \alpha_d^{1/2} |\Delta p|^{1/2} \quad (9)$$

$$\Gamma_d = \text{sign}(\Delta p) \cdot 3,85 \cdot \frac{\rho_d}{\sqrt{\rho_c}} N'''^{1/3} \alpha_d^{1/2} |\Delta p|^{1/2} \quad (10)$$

Where the effective pressure difference equals:

$$\Delta p = p_{sat} - \left( p - C_E \frac{2}{3} \rho_c k_c \right) \quad (11)$$

$C_E$  is the Egler coefficient, which varies between 1 and 1,4.  $C_{CR}$  is the condensation reduction factor.  $N'''$  is the bubble number density, which is calculated with assumed diminishing linear ramp:

$$N''' \begin{cases} N_0''' & \alpha_d \leq 0,5 \\ 2(N_0''' - 1)(1 - \alpha_d) + 1 & \alpha_d > 0,5 \end{cases} \quad (12)$$

Where  $N_0'''$  represents the initial value of the bubble number density.

Interfacial momentum exchange term is defined with:

$$M_c = C_d \frac{1}{8} \rho_c A_i''' |v_r| v_r + C_{TD} \rho_c k_c \nabla \alpha_d = -M_d \quad (13)$$

## Numerical models

Numerical analyses were taken by using the CFD program FIRE.

### Computation model

To analyse the flow characteristics of the in-nozzle flow different nozzle models were made. Since some analysis shown, that the pressure drop in nozzle is significant only in the area of the needle seat, sac chamber and nozzle holes, the meshes were modelled only for the above mentioned parts. For the maximal needle lift of 0,35 mm, two different nozzle models, representing real size and one half of the nozzle were made. First analyses show no significant changes between the results of the real size and one half model. For this reason we used one half model in further research.

### ***Initial and boundary conditions***

When analysing steady state flow, pressure boundary conditions at the inlet and outlet are specified. The fluids used for analysis are the diesel D2 and biodiesel B100, with the temperature of 293,15 K, the density 825 kg/m<sup>3</sup> for D2 and 875 kg/m<sup>3</sup> for B100 and dynamic viscosity of 2,45 mm<sup>2</sup>/s for D2 and 2,6 mm<sup>2</sup>/s for B100. K-ε turbulence model is employed. In all simulations the fuel was considered to be incompressible. Since the maximal velocities of fuel are much smaller (less than 50%) than the velocity of sound we believe this assumption is correct.

### **Used types of meshes and their various density**

Numerical analysis includes various densities and types of meshes. Densities and their related type of used meshes are presented in Table 2 in Figure 1. Standard approach is to use block-structured types of meshes, while we had a chance to compare (time) it with structured, to study the differences between them.

**Table 2.** Various densities and related types of meshes

Name	Number of used elements	Type
mesh 1	21.440	structured
mesh 2	41.920	structured
mesh 3	162.050	structured
mesh 4	241.240	structured
mesh 5	376.960	structured
mesh 6	610.750	structured
mesh 7	39.000	block- structured
mesh 8	95.000	block- structured
mesh 9	319.360	block- structured
mesh 10	505.760	block- structured

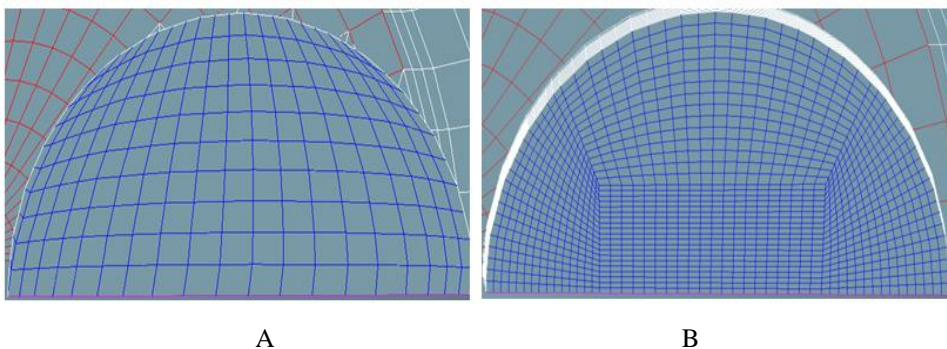


**Figure 1:** Structured (A) and block- structured (B) types of used meshes

## RESULTS

Results were taken on two different positions on the injector hole. The positions are presented on the Figure 2.

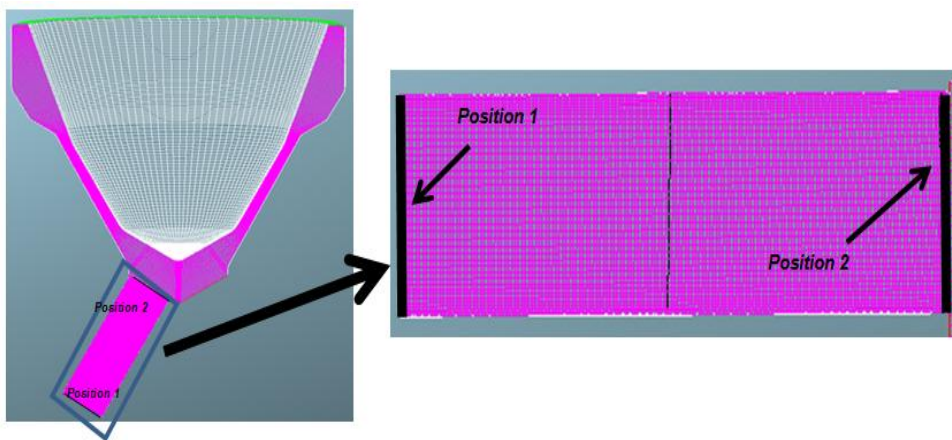


*Figure 2: Positions of point were the result are taken*

Velocity profiles and volume fraction distributions derived from the CFD analyses for different meshed models are presented on following figures. Figures 3-6 show the results of volume fraction distribution in nozzle hole with various mesh densities.

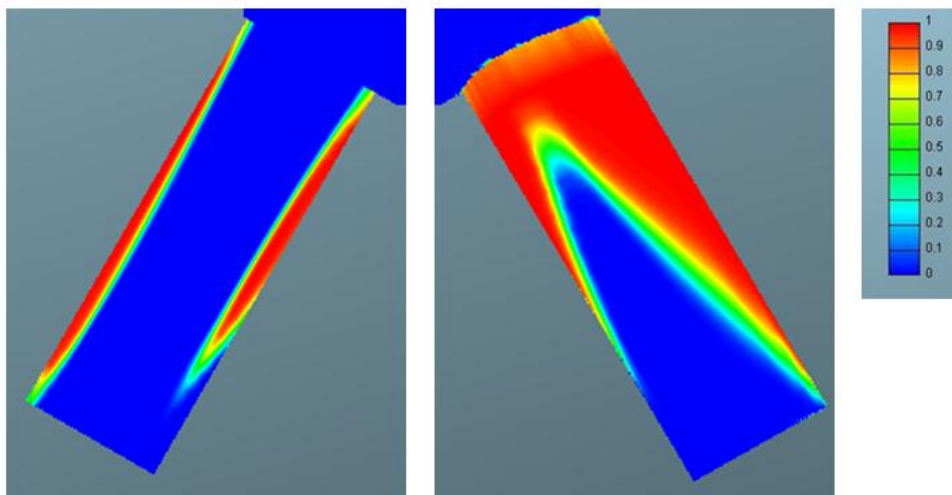


*Figure 3: Volume fraction (mesh 7)*

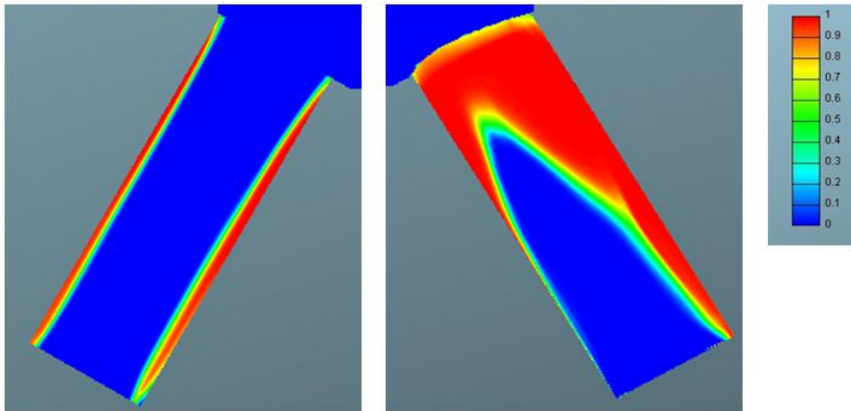


**Figure 4:** Volume fraction (mesh 8)

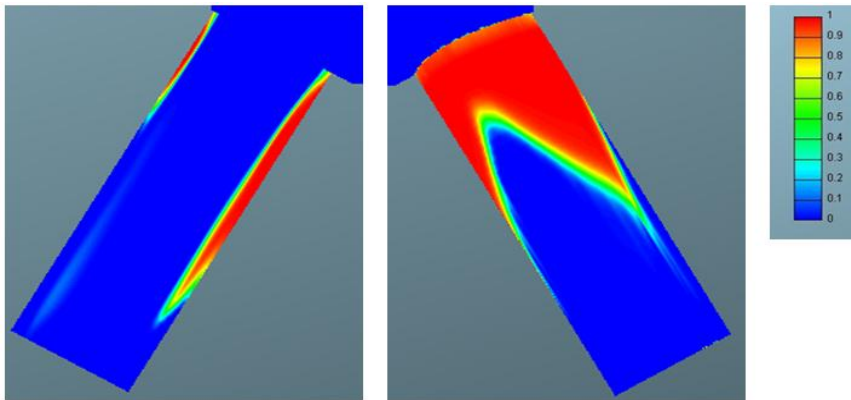


**Figure 5:** Volume fraction (mesh 9)

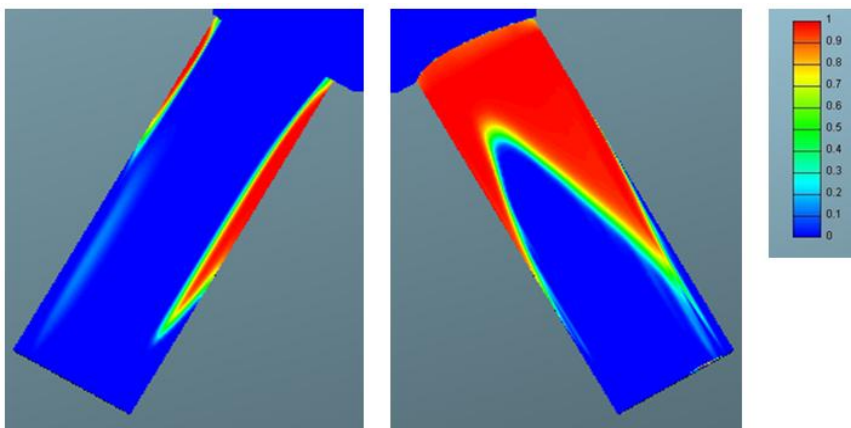


**Figure 6:** Volume fraction (mesh 10)

The velocity profiles and volume fraction distributions in nozzle holes with various densities, figures 3-6 are almost identical. The results indicate already known fact that the outflow velocity is higher at holes with smaller inclination angles, what results in higher flow coefficient at those holes.

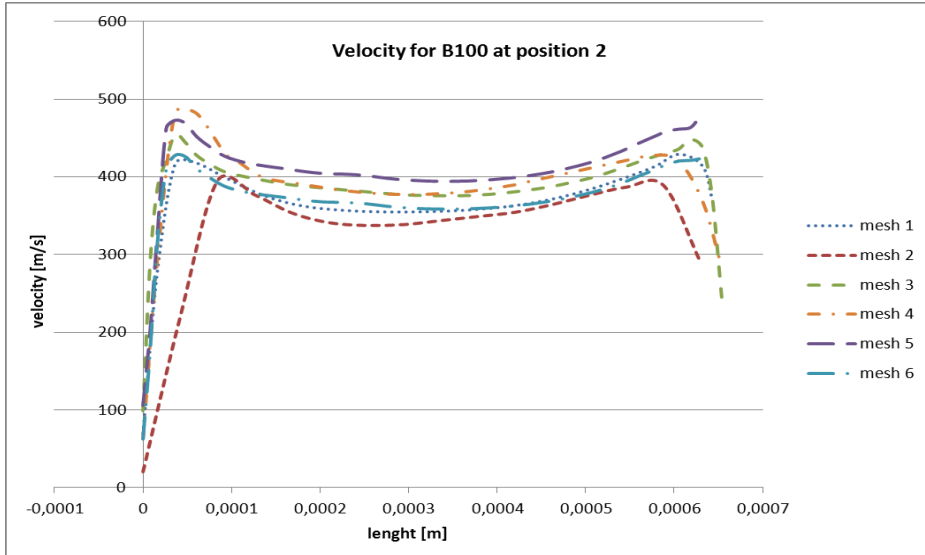


*Figure 7: Velocity profiles for structured type and various densities of used meshes at position 2*

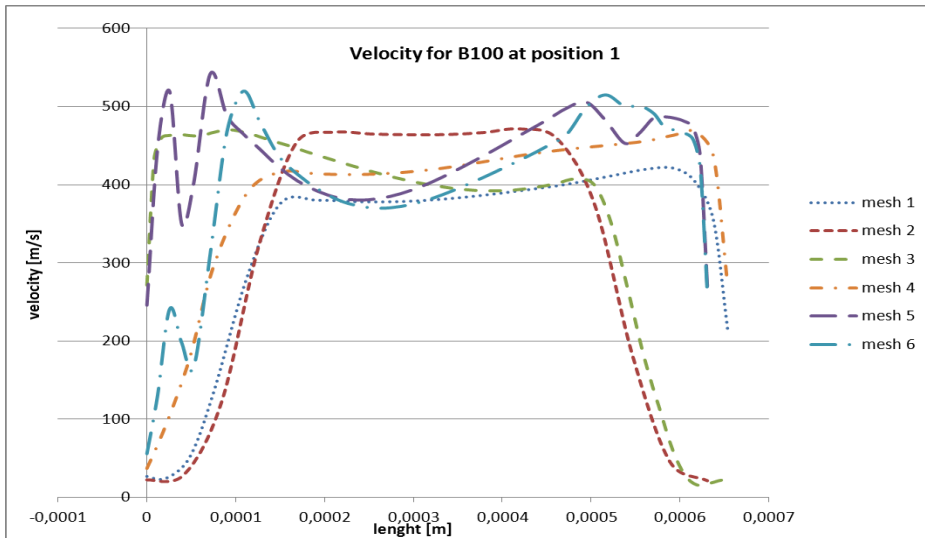


*Figure 8: Velocity profiles for structured type and various densities of used meshes position 1*

The results of the numerical analysis for velocity profiles for structured type and various density are presented on figures 7 and 8, while figure 9 shows the results for block-structured type. From figures 10-12 it is obvious that the numerical result of the volume fraction for structured and block-structured are not significantly different.

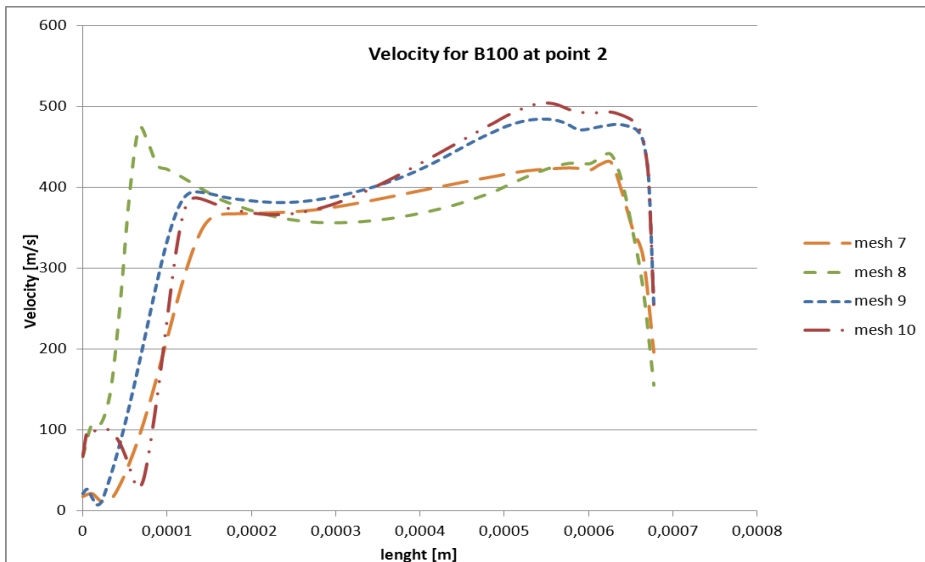


Figure 9: Velocity profiles for block-structured type and various densities of used meshes position 1

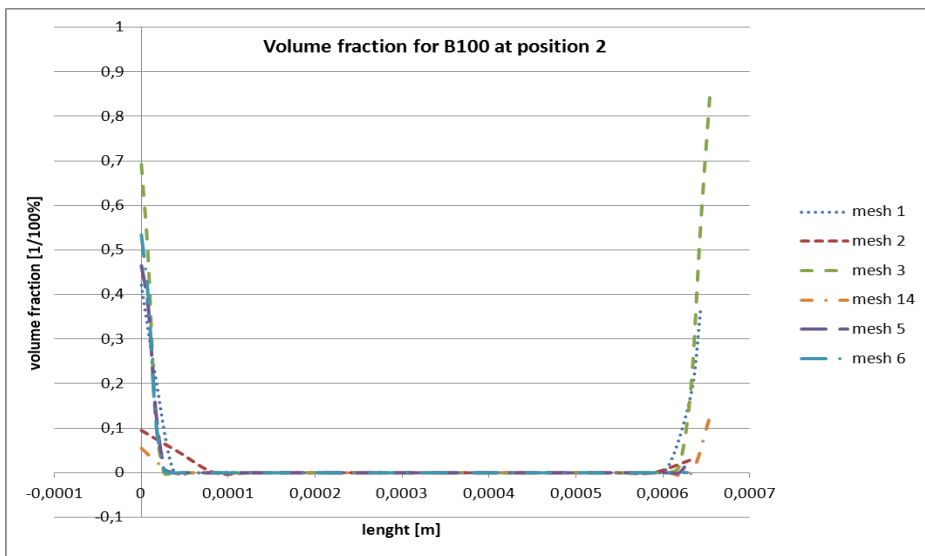
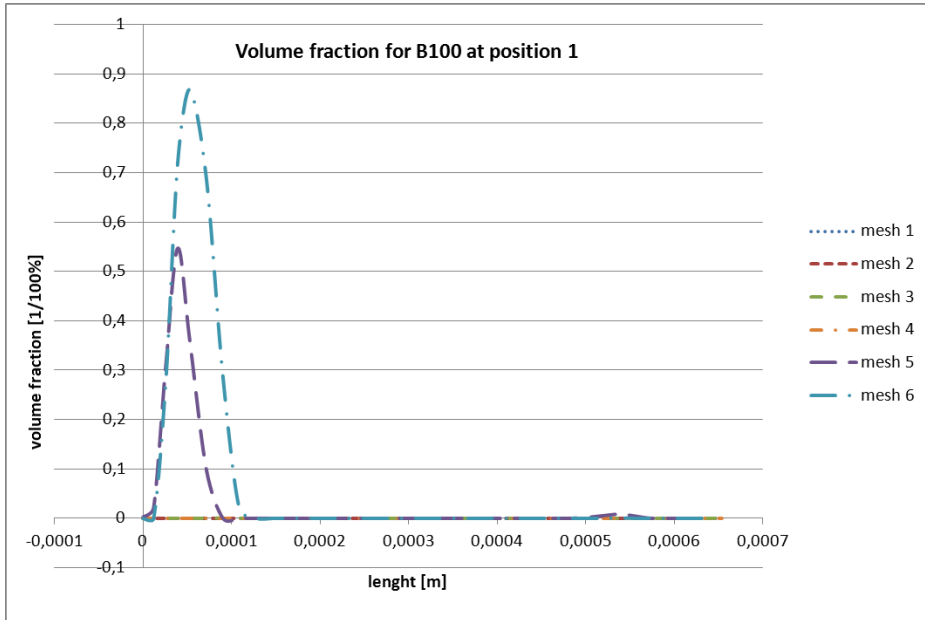
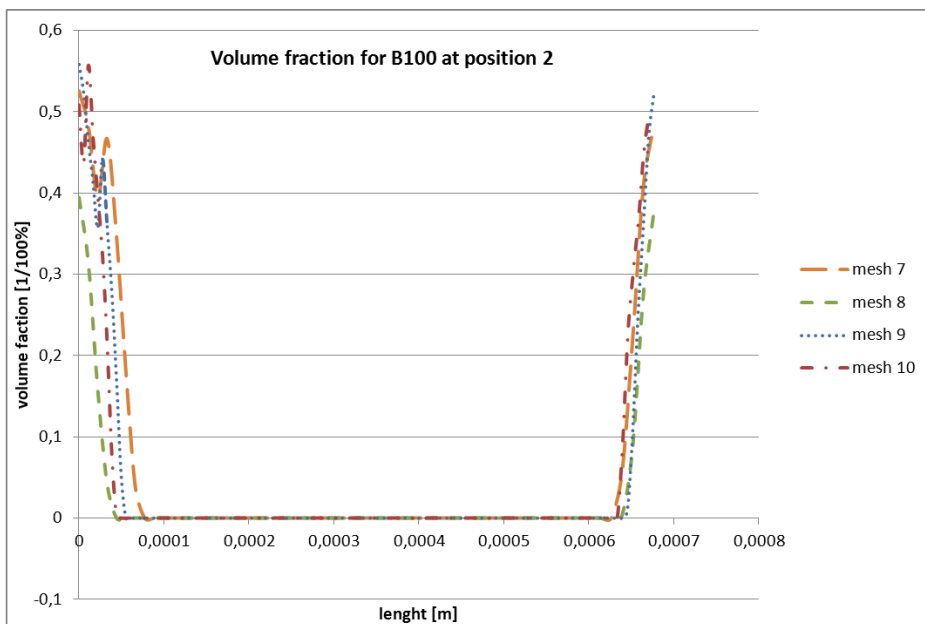


Figure 10: Volume fraction for structured type and various densities of used meshes position 2



*Figure 11: Volume fraction for structured type and various densities of used meshes position 1*



*Figure 12: Volume fraction for block-structured type and various densities of used meshes position 2*

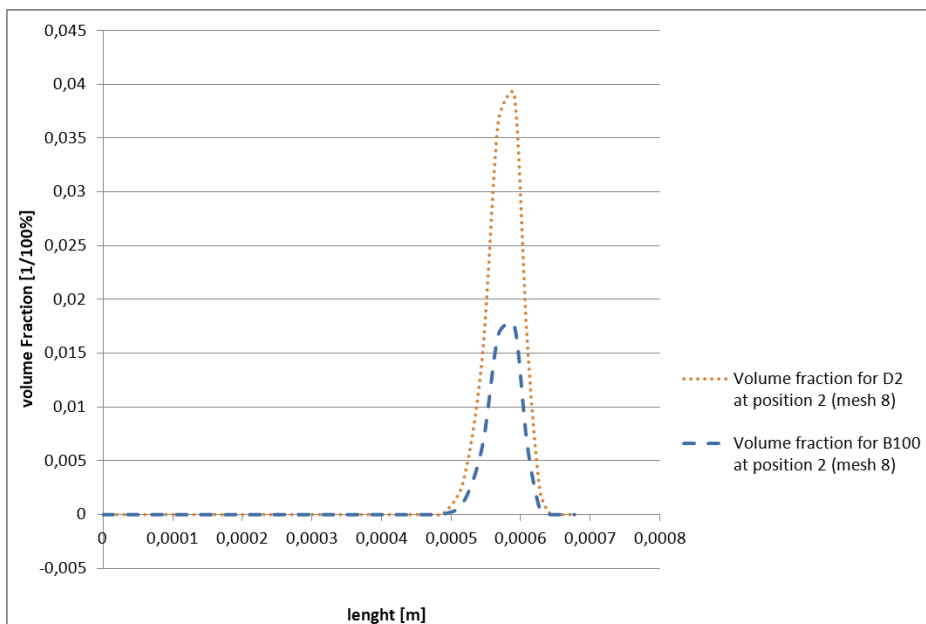


**Figure 13:** Volume fraction for different type of fluid (D2 and B100) at position 2

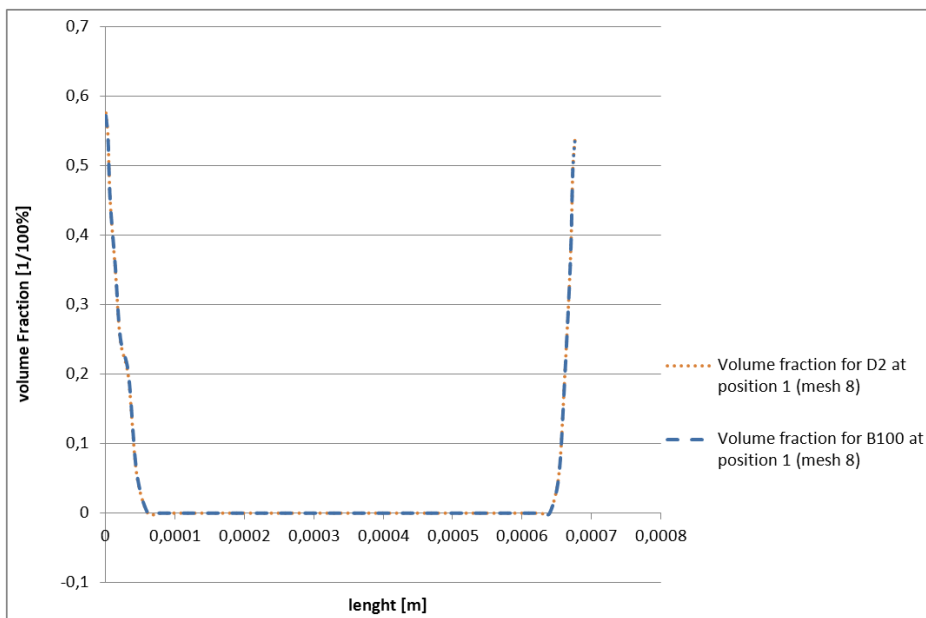


**Figure 14:** Volume fraction for different type of fluid (D2 and B100) at position 1

The results of the numerical analysis show that the block-structured type (figures 7-12) of mesh is better for numerical analysis in nozzle holes. Comparison of the results in Figure 8

an 9 show how different type significantly influences the velocity profiles. When we use structured mesh the velocity profiles are rougher then in case of block-structure. By comparison of result for volume fraction there is no difference between structured and block-structured type of mesh (figure 10-12). When we compare the results for various density meshes there is no significant difference between meshes with higher densities compared to meshes with lower density. The numerical analysis for different type of fluid (D2 and B100) are presented on figures 13-15.

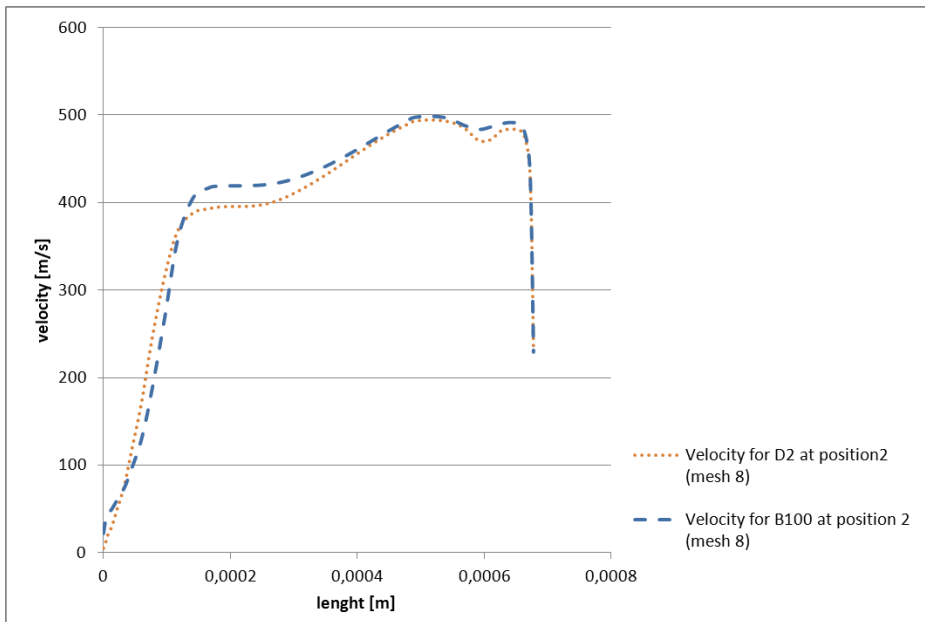


**Figure 15:** Velocity profile for different type of fluid (D2 and B100) at position 2

As already stated the results of influence of different type of fluid (D2 and B100) in nozzle showed no significant difference. Velocity field, velocity profiles and volume fraction distributions on the outlet are comparable. The results are comparable because the density of used fluids is similar and not so much different (difference is about  $50 \text{ kg/m}^3$ ). The difference between dynamic viscosity is also very small and has no effect on the results. Values for mass-flow, viscosity were different (taken from experiment), pressure and temperature were the same for booth fuels.

The differences presented in figures 13-15 are very small. Some volume fraction (indicator for cavitation) analysis were made for different fuels and the difference is even smaller, so it cannot be presented properly in form similar as figures 3-6.

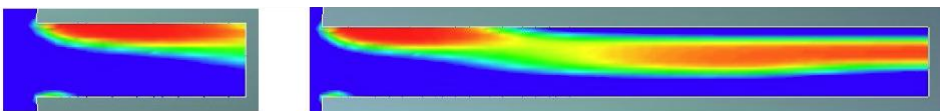


**Figure 16:** Volume fraction in nozzle hole

The vapour fraction for different types of fluid is presented on figure 16. When comparing the results the following could be observed. The structure of the cavitation is not dependent on the length of the nozzle hole. The shape of cavitation in the first part of the hole is almost identical. Later on the vapour cloud is spreading through the hole till it reaches the outlet.

The pressure distributions presented in figure 17 show the very low pressure area in the recirculation zone. This means, that the velocity at the outlet is higher and it is also more uniform. Higher output velocities result also in better atomisation of injected fuel.

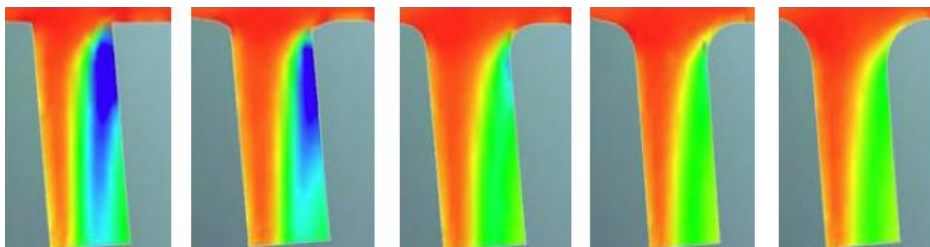


*Figure 17: Pressure distribution in the nozzle hole*

From this first analyses no concrete conclusion could be made. We could only speculate the shorter nozzle hole could have better influence on the spray formation. Further we could also suppose that region where the vapour volume fraction is lowered significantly some damages due to the bubble collapse could be expected.

## CONCLUSIONS

Considering above-mentioned results the following conclusions could be made:

- The numerical analysis shows that higher pressure differences yield more cavitation.
- The results of numerical analysis are comparable for different types of fluid (D2 and B100).
- The numerical result are better when we use block-structured meshes .
- Comparison between structured and block-structured meshes show, that the velocity profiles are much rougher with structured mesh than in case of block-structured meshes.
- To cover all areas of cavitation that could appear in the nozzle hole meshes with higher density should be used .
- By introducing the chamfer at the inlet edges of nozzle hole the cavitation could be lowered significantly.
- First analyses show no significant influence of the nozzle hole length on the shape of the cavitation.

**REFERENCES**

- [1] T. Yoda, T. Tsuda, Influence of injection Nozzle improvement on DI Diesel Engine, SAE paper 970356
- [2] Y.Oishi et.al., A computational Study into the Effect of the Injection Nozzle Inclination Angle on the Flow Characteristics in Nozzle Holes, SAE paper 920580
- [3] C.Arcoumanis et. al., Analysis of the Flow in the Nozzle of a Vertical Multi Hole Diesel Engine Injector, SAE paper 980811
- [4] M.Kato et al., Flow Analysis in Nozzle Hole in Consideration of Cavitation, SAE 970052
- [5] Y.Oishi et.al., A Computational Study into the Effects of the Injection Nozzle Inclination Angle on the Flow Characteristics in the Nozzle Holes, SAE paper 920580
- [6] K.Melcher, J.Chomiak, Experimentelle Untersuchung der Stroemung durch Deseleinspritzduesen in stationaer betriebenen Grossmodel, Bosch Techn.Berichte 5(1976) 4
- [7] ISO-4113:1988, Road Vehicles- Calibration Fluid Diesel Injection Equipment
- [8] H.Hardenberg, Die Nadelhubabhaengigkeit der Durchflussbeiwerte von Lochduessen fuer Direkteinspritzdieselmotoren, MTZ 46(1985) 4, p. 143-146
- [9] FIRE Version 9 – Users manual, Multiphase flow, AVL, 2009
- [10] L.C.Ganippa et.al., The structure of cavitation and its effect on the spray pattern in a single hole diesel nozzle, SAE paper 2001-01-2008
- [11] L.C.Ganippa et.al., Comparison of cavitation phenomena in transparent scaled-up single hole diesel nozzles, 4th international symposium on cavitation, California institute of technology, Pasadena, 2001
- [12] B.Göschel, Einspritzdüsenverschleiß, Forschungvereinigung Verbrennungskraftmaschinen e.V., Heft R245, 1974
- [13] Kavitation. Abschlußberichtüber die Ergebnisse des Schwerpunktprogramm 1966-1972, Deutsche Forschungsgemeinschafts, Boppard, 1974
- [14] G.König et.al., Analysis of flow and cavitation Phenomena in diesel injection nozzles and its effects on spray and mixture formation, 5. Internationales Symposium für Verbrennungsdiagnostik der AVL Deutschland, 6.-7.Juni 2002, Baden Baden, 2002
- [15] C.Arcoumanis et. al., Visualisation of cavitation in diesel engine injectors, Mec.Ind. (2001) 2, 375-381
- [16] C.Arcoumanis et.al., Investigation of cavitation in a vertical multi-hole injector, SAE paper 1999-01-0524
- [17] C.Arcoumanis et.al, Cavitation in real-size multi-hole diesel injector nozzles, SAE paper 2000-01-1249
- [18] C.Badock et.al, Investigation of cavitation in real size diesel injection nozzle, International Journal of Heat and Fluid Flow 20 (1999)
- [19] K.Jung et.al., The breakup characteristics of liquid sheets formed by like-doublet injectors, Journal of Propulsion and Power (sent), <http://rpl.snu.ac.kr/>
- [20] D.Radonjić, Application possibilities of similarity theory and dimensional analysis in designing process of internal combustion engines intake manifold, Mobility and Vehicle Mechanics, Vol. 31, No. 3-4, p.11-31, 2005.